Phase behavior of decamethyl- and octamethylferrocenium salts containing bulky anions: Effects of packing and the anion structure on ionic plastic crystal formation

Mochida, Tomoyuki
Ijiri, Sota
Inoue, Ryota

(Citation)
Journal of Organometallic Chemistry,1040:123828

(Issue Date)
2025-10-01

(Resource Type)
journal article

(Version)
Version of Record

Journal of Organometallic Chemistry 1040 (2025) 123828

Contents lists available at ScienceDirect

Journal of Organometallic Chemistry

journal homepage: www.elsevier.com/locate/jorganchem

Phase behavior of decamethyl- and octamethylferrocenium salts containing bulky anions: Effects of packing and the anion structure on ionic plastic crystal formation

Tomoyuki Mochida [a,b,*], Sota Ijiri [a], Ryota Inoue [a]

[a] Department of Chemistry, Graduate School of Science, Kobe University, 1-1 Rokkodai, Nada, Kobe, Hyogo 657-8501, Japan
[b] Research Center for Membrane and Film Technology, Kobe University, 1-1 Rokkodai, Nada, Kobe, Hyogo 657-8501, Japan

ARTICLE INFO

Keywords:
Ferrocenium salts
Thermal properties
Phase transitions
Ionic plastic crystals
Crystal structures

ABSTRACT

Ionic plastic crystals (IPCs), in which nearly spherical ions undergo rotational motion in the solid state, have recently attracted attention because of their unique properties. To investigate the ability of bulky anions to induce IPC formation in organometallic salts, we prepared decamethylferrocenium salts ([**1**]X) and octamethylferrocenium salts ([**2**]X) containing a $CB_{11}H_{12}^-$ carborane anion or a hexafluoropropane-1,3-disulfonamide anion ($CPFSA^-$), of which [**2**]CPFSA was previously reported. Although all the salts underwent a solid–solid phase transition, only [**1**]$CB_{11}H_{12}$ formed an IPC phase above 494 K. This phase behavior correlated with the low-temperature crystal structures; [**1**]$CB_{11}H_{12}$ and [**2**]$CB_{11}H_{12}$ both adopted alternating cation–anion packing arrangements favorable for IPC formation, but the local cation–anion configuration of the latter hindered molecular rotation. In contrast, [**1**]CPFSA and [**2**]CPFSA adopted non-alternating cation–anion arrangements because of ion pairing induced by charge localization within the anion structure and face-to-face interactions between cation ligands. Thus, molecular properties, local cation–anion configurations, and packing arrangements influence IPC formation.

1. Introduction

Ionic plastic crystals (IPCs) are solid-state materials in which nearly spherical ions undergo dynamic rotational motion; this type of phase is often observed in salts containing spherical cations, typically quaternary ammonium salts [1–7]. The ionic conduction [1–5], ferroelectricity [8–13], phase transitions [6,7,14–20], and thermal properties [21] of these materials have been extensively studied.

Several metallocenium salts, such as PF_6^- salts of ferrocene, cobaltocene, and octamethylferrocene, also form IPCs owing to the nearly globular shape of their cations [22–24]. Metallocenium salts are particularly intriguing because of their magnetic properties [25] and the barocaloric effects associated with IPC phase transitions [26]. However, unlike quaternary ammonium salts, most metallocenium salts form IPC phases only at elevated temperatures, which impedes their application as ionic conductors and limits detailed studies of their physical properties. This tendency is likely associated with their relatively large molecular weights and high symmetry. In contrast, the high phase transition temperature (Tc) of these materials facilitates crystallographic analysis, enabling the elucidation of the relationship between the molecular structure and the Tc associated with IPC formation. We previously examined the phase behavior of various metallocenium salts and observed the following tendencies about the phase transitions of decamethyl- and octamethylferrocenium salts with various anions ([**1**]X and [**2**]X, respectively; Fig. 1a): (i) The Tc of [**2**]X was typically 70–100 K lower than that of [**1**]X with identical anions (e.g., T_C = 398 and 319 K for [**1**]Tf_2N and [**2**]Tf_2N, respectively; Tf_2N = $(SO_2CF_3)_2N^-$) [27,28]. (ii) Larger anions resulted in lower T_C values, as observed for [**2**]X (X = BF_4^-, PF_6^-, $CF_3BF_3^-$, $CF_3SO_3^-$, $CH_2BrBF_3^-$, $FeCl_4^-$, $GaCl_4^-$, $N(SO_2F)_2^-$, $B(CN)_4^-$, and Tf_2N^-) [25,27,28], although this correlation was not observed in metallocenium salts with smaller cations [29]. (iii) Non-alternating cation–anion crystal arrangements hindered IPC formation [25], as also observed in other metallocenium salts [29–31] and onium salts [14]. These findings are expected to be useful for the molecular design of IPCs.

These results suggested that large, bulky anions with spherical or quasi-spherical shapes can effectively induce IPC formation at lower temperatures. To test this hypothesis, in the present study, we prepared

* Corresponding author at: Department of Chemistry, Graduate School of Science, Kobe University, 1-1 Rokkodai, Nada, Kobe, Hyogo 657-8501, Japan.
E-mail address: tmochida@platinum.kobe-u.ac.jp (T. Mochida).

https://doi.org/10.1016/j.jorganchem.2025.123828
Received 15 May 2025; Received in revised form 25 July 2025; Accepted 18 August 2025
Available online 20 August 2025

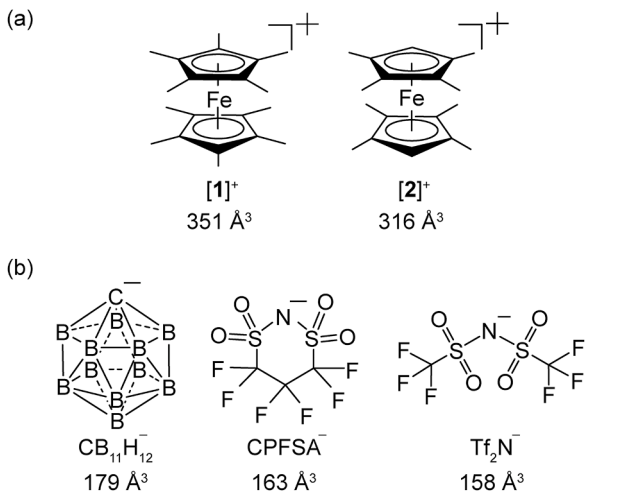

Fig. 1. Structural formulas of the (a) cations and (b) anions investigated in this study. The van der Waals volume of each molecule estimated via DFT calculations is indicated below the structure. [**2**]CPFSA, [**1**]Tf_2N, and [**2**]Tf_2N were previously reported [25,27].

[**1**]X and [**2**]X using two bulky anions: the carborane anion ($CB_{11}H_{12}^-$) and the quasi-spherical hexafluoropropane-1,3-disulfonamide anion ($CPFSA^-$; Fig. 1b). The salt [**2**]CPFSA had been reported previously [25]. We examined their phase behavior and crystal structures. Organometallic [29] and quaternary ammonium [32] salts of the carborane anion $CB_{11}H_{12}^-$ have been shown to form IPC phases at elevated temperatures. $CPFSA^-$, a cyclic anion with a molecular volume comparable to that of Tf_2N, has been reported to readily form IPC phases with onium cations [33,34], whereas [**2**]CPFSA did not form an IPC phase, likely because of its non-alternating cation–anion crystal arrangement [25]. Although all the salts prepared in this study underwent phase transitions, only [**1**]$CB_{11}H_{12}$ formed an IPC phase at high temperatures, and the factors affecting their phase behavior are discussed below in terms of structural data.

2. Results and discussion

2.1. Phase behavior

[**1**]X (X = $CB_{11}H_{12}^-$, $CPFSA^-$) and [**2**]$CB_{11}H_{12}$ were prepared as green crystals via anion exchange reactions from their corresponding chloride salts, and their phase sequences were determined by differential scanning calorimetry (DSC, Fig. S1 and Fig. 2). The data shown for [**2**]CPFSA were obtained from the literature [25]. The highest-temperature phase in the diagram is referred to as phase I. The *Tc* associated with the formation of phase I and the structural features of [**1**]X (X = $CB_{11}H_{12}$, CPFSA, and Tf_2N [27]) are summarized in Table 1.

[**1**]$CB_{11}H_{12}$ formed an IPC phase at 494.2 K ($\Delta S = 32.5$ J mol^{-1} K^{-1}). Notably, its *Tc* was significantly higher than that of [**1**]Tf_2N (*Tc* = 398 K) [27], despite the larger anion size. The transition to the IPC phase was confirmed by the loss of birefringence observed via polarized optical microscopy. In contrast, [**2**]$CB_{11}H_{12}$ underwent a solid–solid phase transition at 301.0 K ($\Delta S = 27.3$ mol^{-1} K^{-1}) but did not lose birefringence, indicating that phase I was not an IPC phase. The low-symmetry, non-IPC crystal structure of [**2**]$CB_{11}H_{12}$ in phase I was also confirmed by powder X-ray diffraction (PXRD). Similarly [**1**]CPFSA underwent a phase transition at 397.1 K ($\Delta S = 47.1$ mol^{-1} K^{-1}), but its phase I was not an IPC phase. None of these salts underwent melting; hence, their melting entropies were not determined. [**2**]CPFSA underwent two phase transitions at 255 K ($\Delta S = 9.9$ J mol^{-1} K^{-1}) and 316 K ($\Delta S = 67.3$ J mol^{-1} K^{-1}) without forming an IPC phase [25]. Thus, the phase behavior of [**1**]X and [**2**]X prepared in this study differed significantly

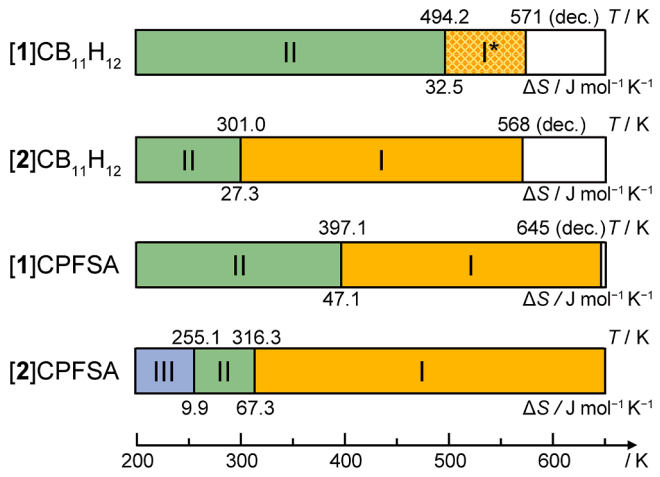

Fig. 2. Phase sequences of [**1**]X and [**2**]X (X = $CB_{11}H_{12}^-$, $CPFSA^-$). The data presented for [**2**]CPFSA were obtained from the literature [25]. The *Tc* values (K) and corresponding transition entropies (J mol^{-1} K^{-1}) are indicated above and below each bar chart, respectively. The asterisk denotes an IPC phase.

from each other, in contrast to the salts with X = BF_4^-, PF_6^-, $CF_3SO_3^-$, and Tf_2N^-, which exhibited similar phase sequences including IPC phases [27].

Thermogravimetric analysis (TGA) under a nitrogen atmosphere (scan rate: 3 K min^{-1}; Fig. S2) revealed high decomposition temperatures (corresponding to a 3wt % weight loss) of 571, 568, and 645 K for [**1**]$CB_{11}H_{12}$, [**2**]$CB_{11}H_{12}$, and [**1**]CPFSA, respectively, reflecting the thermal stabilities of the anions.

2.2. Crystal structures

The crystal structures of [**1**]$CB_{11}H_{12}$ [**2**]$CB_{11}H_{12}$, and [**1**]CPFSA in phase II (low-temperature phase) were determined at 293 K, 90 K, and 90 K, respectively. Their packing diagrams and the structure of [**2**]CPFSA [25] are shown in Fig. 3. [**1**]$CB_{11}H_{12}$ and [**2**]$CB_{11}H_{12}$ adopted alternating cation–anion structures, whereas [**1**]CPFSA and [**2**]CPFSA did not.

In the packing diagram of [**1**]$CB_{11}H_{12}$, which crystallized in space group *P2/m* (*Z* = 1), the cation was at the center of the unit cell surrounded by eight anions at the apexes, indicating a coordination number of eight (Fig. 3a) [35]. The radius ratio ρ ($= r_{anion}/r_{cation}$) of this salt was estimated to be 0.80 based on the molecular volume, exceeding 0.73. Therefore, the coordination number is consistent with the radius ratio rule for inorganic salts [36]. The carbon atom in the anion was disordered over two opposite sites, with carbon and boron occupancies of 0.5 each. The distances between the carbon atoms and neighboring boron atoms ranged from 1.733(4) to 1.747(5) Å, consistent with the average B–C (1.69–1.70 Å) and B–B (1.77–1.78 Å) bond lengths in $CB_{11}H_{12}^-$ [37].

[**2**]$CB_{11}H_{12}$ crystallized in space group *C2/c*, and its packing diagram is shown in Fig. 3b (*Z* = 4). This salt exhibited extensive disorder. The cation was positionally disordered over two sites with occupancies of 0.61 and 0.39 (Fig. S3). The anion also showed orientational disorder over two positions, and because of this extensive disorder, the carbon atom was tentatively modeled as being disordered over all positions. As in [**1**]$CB_{11}H_{12}$, the cations and anions in this salt adopted an alternating arrangement, but the unit cell differed significantly. The radius ratio for this salt was estimated to be 0.83 based on the molecular volume, for which the radius ratio rule predicts a coordination number of eight. However, each cation was surrounded by seven anions (Fig. 3b, right): four anions in the same *ac* plane (denoted as A in the figure), two on one side of the plane (denoted as B), and one on the other side (denoted as C). The center-to-center distances between the cation and surrounding anions were 6.99–7.40 Å for A, 8.27 Å for B, and 6.23 Å for C, with C

Table 1
The phase transition temperature to phase I (*Tc*), the molecular arrangement and coordination number (CN) in phase II, and the radius ratio of [**1**1]X (X = $CB_{11}H_{12}^-$, $CPFSA^-$, and Tf_2N^-).

	phase I	*Tc*/K	cation–anion arrangement	cation–cation arrangement	CN	ρ [c]
[**1**]$CB_{11}H_{12}$	IPC	494.2	alternating	–	8	0.80
[**2**]$CB_{11}H_{12}$	non-IPC	(301.0)[d]	alternating	–	7	0.83
[**1**]CPFSA	non-IPC	(397.1)[d]	non-alternating	dimeric	–	0.77
[**2**]CPFSA[a]	non-IPC	(316.3)[d]	non-alternating	columnar	–	0.80
[**1**]Tf_2N[b]	IPC	398.1	alternating	–	8	0.77
[**2**]Tf_2N[b]	IPC	318.6	alternating	–	6	0.79

[a] Ref. 25. [b]Ref. 27. [c]Radius ratio (r_{anion}/r_{cation}) estimated via DFT calculations. [d]Phase transition to the non-IPC phase.

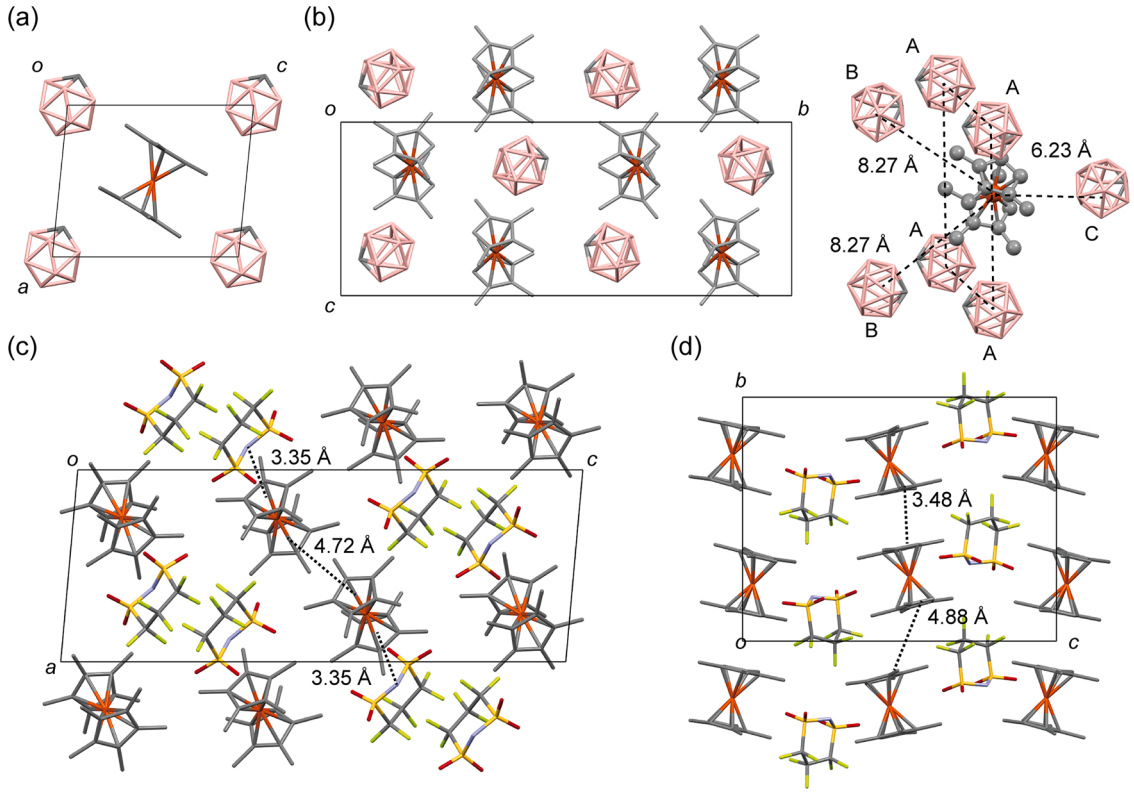

Fig. 3. Packing diagrams of (a) [**1**]$CB_{11}H_{12}$ (293 K), (b) [**2**]$CB_{11}H_{12}$ (90 K), (c) [**1**]CPFSA (90 K), and (d) [**2**]CPFSA (100 K [25]). In (b), the arrangement of the anions surrounding the cation is illustrated on the right. Hydrogen atoms were omitted for clarity, and in (a) and (b), one of the disordered components of the molecules was omitted. The intermolecular distances are indicated in the figures (see text).

being notably closer. This is because anion C is located at the concave site of the cation, where no methyl groups are present. Therefore, the absence of an IPC phase in this compound likely resulted from this local anion–cation configuration, which restricted the molecular rotation because of steric hindrance. This situation resembles that of [Ru(Cp)(C_6H_6)]$SbCl_6$ (Cp = $C_5H_5^-$), where the anions are sterically fixed between the cations, thus hindering IPC formation [38].

[**1**]CPFSA crystallized in space group $P2_1/n$ ($Z = 4$), and its packing diagram is shown in Fig. 3c. In this salt, the cations formed dimers via face-to-face interactions between the Cp* rings (Cp* = $C_5Me_5^-$), with a centroid-to-centroid distance of 4.72 Å. The anions were adjacent to the outer Cp* rings of the dimer, with $(SO_2)_2N^-$ moieties contacting each Cp* ring ($Cp^*_{centroid}$–N distance: 3.35 Å). In contrast, [**2**]CPFSA adopted a segregated stacking arrangement of cations and anions (Fig. 3d), with cations forming columnar arrangements via face-to-face interactions between the cyclic ligands. The N atom of the anion was near the Fe center of the cation. The absence of an IPC phase in these salts was consistent with their non-alternating cation–anion arrangements.

2.3. Molecular arrangements

The formation of IPC phases and the molecular arrangements of [**1**]X and [**2**]X (X = $CB_{11}H_{12}^-$, $CPFSA^-$, and Tf_2N^- [27]) are summarized in Table 1. The IPC phases in these salts are discussed below in terms of their structural features.

The packing structures of these salts depended strongly on the anions. As described in the previous section, the $CB_{11}H_{12}$ salts adopted alternating cation–anion arrangements, which was attributed to the spherical shape and delocalized negative charge of the anion. Similarly, Tf_2N salts adopted alternating molecular arrangements [27]. In contrast, the CPFSA salts adopted non-alternating arrangements, possibly due to the anion's deviation from a spherical shape, and the localization of negative charge mainly on the nitrogen atoms, which could promote ion pairing with the cation [30]. Indeed, in the crystal structure, the nitrogen atom of the anion was positioned near the Cp ligand or the Fe center of the cation. Face-to-face interactions between the Cp* or C_5Me_4H ligands, which led to dimeric or columnar cation arrangements, also facilitated the adoption of non-alternating arrangements in these salts. However, such interactions are less likely with organometallic cations

with smaller Cp ligands; for example, [Ru(Cp)(C_6H_6)]CPFSA adopted an alternating molecular arrangement [38], and CPFSA salts of half-sandwich CpRu complexes exhibited both alternating and non-alternating cation–anion arrangements [38,39].

The effects of packing arrangements on the formation of IPC phases, as reported in previous studies and observed in the present work, are summarized as follows: (i) Non-alternating cation–anion arrangements hinder IPC formation [25,29–31], as also observed in the current study. In addition, the symmetry of the cation–anion arrangements affects the *T*c of salts with alternating molecular arrangements [38,39]. (ii) Local cation–anion interactions sterically restrict molecular rotation, thereby suppressing IPC phase formation [38], as also observed in [**2**]$CB_{11}H_{12}$. (iii) The anion size significantly affects the *T*c values. A decrease in the *T*c associated with the IPC phase with increasing anion size (or radius ratio ρ) is reported for [**1**]X and [**2**]X [25]. However, the present salts with $CPFSA^-$ and $CB_{11}H_{12}^-$ deviated from this trend, as discussed below.

This study revealed that the $CB_{11}H_{12}^-$ anion did not effectively induce IPC formation at low temperatures, despite its spherical shape and large volume [**1**]$CB_{11}H_{12}$ (ρ = 0.80) exhibited a much higher *T*c (494.2 K) than [**1**]Tf_2N (ρ = 0.77, *T*c = 398 K). Similarly, [Ru(Cp)(C_6H_6)]$CB_{11}H_{12}$ and [$CoCp_2$]$CB_{11}H_{12}$ exhibited high *T*c values of 501 K and 402 K, respectively [29], and even the quaternary salts of $CB_{11}H_{12}$ exhibited rather high *T*c values [32]. The reason for these observations remains unclear, but possible factors include the excessively large volume and abundant peripheral hydrogen atoms of this atom that may sterically hinder molecular rotation. Although quaternary salts of the CPFSA anion readily form IPC phases, salts of sandwich or half-sandwich cations with this anion failed to form IPC phases when the cation–anion arrangement was non-alternating, as observed in this study, and exhibited IPC phases only at elevated temperatures when the arrangement was alternating [38,39]. These results suggest that this anion is less effective at inducing IPC formation in organometallic ionic crystals even though its molecular volume is comparable to that of Tf_2N^-.

3. Conclusion

In this study, we investigated the phase behavior and crystal structures of decamethyl- and octamethylferrocenium salts containing bulky anions to evaluate the tendency of these materials to form IPC phases. Of the four salts examined, only [**1**]$CB_{11}H_{12}$ formed an IPC phase, and its *T*c was higher than those of previously reported salts containing different anions. This finding is consistent with our previous observations that the $CB_{11}H_{12}^-$ anion, despite being nearly spherical and bulky, is less effective for IPC formation. Moreover, the corresponding octamethyl salt, [**2**]$CB_{11}H_{12}$, did not form an IPC phase, likely because the local cation–anion configuration in the crystal hindered molecular rotation [**1**]CPFSA and [**2**]CPFSA also did not form IPC phases, likely because both adopted non-alternating cation–anion packing arrangements as a result of cation–anion ion pairing and face-to-face interactions between cation ligands. Although previous studies have shown that increasing the anion size decreases the *T*c and promotes IPC formation, the present results indicated that $CB_{11}H_{12}^-$ and $CPFSA^-$ anions are less effective at inducing IPC formation, despite their large volumes. This study provided further evidence that IPC formation depends on (i) molecular properties such as size, shape, and charge distribution, (ii) local cation–anion configurations, and (iii) packing arrangements, such as alternating and non-alternating. These findings provide useful insights for the molecular design of both organometallic IPCs and organic IPCs containing onium cations.

4. Experimental section

4.1. General methods

Decamethylferrocene (> 97 %) and octamethylferrocene were purchased from Sigma-Aldrich. Lithium 1,1,2,2,3,3-hexafluoropropane-1,3-disulfonimide (Li[CPFSA], > 98.0 %) was obtained from Tokyo Chemical Industry Co. (TCI), and cesium carborane ($Cs[CB_{11}H_{12}]$) was purchased from Strem Chemicals, Inc. FT-IR spectra were recorded on a Thermo Nicolet iS5 FT-IR spectrometer equipped with an attenuated total reflectance (ATR) accessory (diamond). DSC was performed using a TA Instruments Q100 calorimeter with aluminum hermetic pans at a heating rate of 10 K min^{-1}. TG–DTA was carried out on a Rigaku TG8120 analyzer with aluminum sample pans under a nitrogen atmosphere at a heating rate of 3 K min^{-1}. Variable-temperature PXRD measurements were performed using a Rigaku XtaLAB Synergy-S diffractometer with Cu Kα radiation. The molecular van der Waals volumes of the samples were estimated via DFT calculations (ωB97-D/LanL2DZ, Spartan '24), and then equivalent sphere radii were derived.

4.2. Synthesis of [Fe(C_5Me_5)$_2$]$CB_{11}H_{12}$ ([**1**]$CB_{11}H_{12}$)

SO_2Cl_2 (0.03 mL, 0.38 mmol) was added to an [Fe(Cp*)$_2$] solution (80 mg, 0.25 mmol) in dichloromethane (1 mL) under a nitrogen atmosphere, and the resulting solution was stirred for 15 min. Next, the solvent was removed under reduced pressure, and the resulting residue was dried under vacuum. This solid was then dissolved in water (3.5 mL), and an aqueous $Cs[CB_{11}H_{12}]$ solution (89 mg, 0.32 mmol, 2.5 mL) was added dropwise with stirring. After this mixture was stirred for 30 min, the precipitate that formed was collected by filtration and dried under vacuum. This crude product was then dissolved in dichloromethane and filtered through a cotton plug, and the filtrate was isolated by evaporation and dried under vacuum. Recrystallization from acetone/diethyl ether by slow cooling (–40 °C) afforded green crystals (70 mg, 61 % yield). FT-IR (ATR, cm^{-1}): 571, 604, 688, 715, 750, 790, 869, 942, 980, 1019, 1062, 1086, 1336, 1383, 1423, 1447, 1470, 2535, 2916, 2958, 2981, 3081. Anal. Calcd for $C_{21}H_{42}B_{11}Fe$: C, 53.74; H, 9.02; N, 0.00. Found: C, 54.02; H, 8.96; N, 0.06.

4.3. Synthesis of [Fe(C_5Me_4H)$_2$]$CB_{11}H_{12}$ ([**2**]$CB_{11}H_{12}$)

[**2**]$CB_{11}H_{12}$ was synthesized from [Fe(C_5Me_4H)$_2$] (77 mg, 0.26 mmol), SO_2Cl_2 (0.04 mL, 0.50 mmol), and $Cs[CB_{11}H_{12}]$ (91 mg, 0.33 mmol), following the same procedure used for [**1**]$CB_{11}H_{12}$. Green crystals were obtained (58 mg, 51 % yield). FT-IR (ATR, cm^{-1}): 565, 608, 689, 716, 750, 789, 869, 945, 980, 1019, 1063, 1086, 1337, 1383, 1423, 1447, 1470, 1955, 2037, 2535, 2916, 2959, 2981, 3082. Anal. Calcd for $C_{19}H_{38}B_{11}Fe$: C, 51.72; H, 8.68; N, 0.00. Found: C, 50.35; H, 8.32; N, 0.29.

4.4. Synthesis of [Fe(C_5Me_5)$_2$]CPFSA ([**1**]CPFSA)

[**1**]CPFSA was synthesized from [Fe(Cp*)$_2$] (79 mg, 0.24 mmol), SO_2Cl_2 (0.03 mL, 0.38 mmol), and Li[CPFSA] (95 mg, 0.32 mmol, in 3 mL of water), following the same procedure used for [**1**]$CB_{11}H_{12}$. Green crystals were obtained (126 mg, 84 % yield). FT-IR (ATR, cm^{-1}): 575, 604, 646, 669, 797, 903, 997, 1025, 1039, 1087, 1155, 1217, 1257, 1280, 1331, 1347, 1380, 1427, 1455, 1477, 2917, 2957. Anal. Calcd for $C_{23}H_{30}NO_4F_6S_2Fe$: C, 44.67; H, 4.89; N, 2.26. Found: C, 44.64; H, 5.13; N, 2.19.

4.5. X-Ray crystal structure determination

Single crystals of [**1**]$CB_{11}H_{12}$ were obtained by recrystallization from an acetone/diethyl ether mixture via slow cooling (–40 °C), crystals of [**2**]$CB_{11}H_{12}$ were obtained by evaporation of a dichloromethane/hexane solution, and crystals of [**1**]CPFSA were obtained by diffusing diethyl ether into an acetone solution (−6 °C). Single-crystal X-ray diffraction of [**1**]$CB_{11}H_{12}$ was collected using a Bruker APEX II Ultra diffractometer (Mo Kα radiation) at 293 K, whereas for [**2**]$CB_{11}H_{12}$ and [**1**]CPFSA, a Rigaku XtaLAB Synergy-S diffractometer (Cu Kα radiation) at 90 K was used. Structure solution and refinement were performed using SHELXL

[40] and Olex2 [41–43]. The crystallographic data are presented in Table S1. The CCDC deposition numbers are 2373890 ([**1**]$CB_{11}H_{12}$), 2448389 ([**2**]$CB_{11}H_{12}$), and 2448057 ([**1**]CPFSA).

CRediT authorship contribution statement

Tomoyuki Mochida: Writing – review & editing, Writing – original draft, Supervision, Investigation, Conceptualization. **Sota Ijiri:** Writing – original draft, Visualization, Investigation. **Ryota Inoue:** Visualization, Investigation.

Declaration of competing interest

The authors declare no conflict of interest.

Acknowledgment

This work was financially supported by KAKENHI (grant number: 24K01497) from the Japan Society for the Promotion of Science (JSPS) and a Grant-in-Aid for JSPS Research Fellows (grant number: 25KJ1806). We are grateful to Research Facility Center for Science and Technology of Kobe University for supporting the experiments.

Supplementary materials

Supplementary material associated with this article can be found, in the online version, at doi:10.1016/j.jorganchem.2025.123828.

Data availability

Data will be made available on request.

References

[1] S. Das, A. Mondal, C.M. Reddy, Harnessing molecular rotations in plastic crystals: a holistic view for crystal engineering of adaptive soft materials, Chem. Soc. Rev. 49 (2020) 8878–8896.
[2] D.R. MacFarlane, J. Huang, M. Forsyth, Lithium-doped plastic crystal electrolytes exhibiting fast ion conduction for secondary batteries, Nature 402 (1999) 792–794.
[3] H. Zhu, D.R. MacFarlane, J.M. Pringle, M. Forsyth, Organic ionic plastic crystals as solid-state electrolytes, Trends Chem. 1 (2019) 126–140.
[4] M.L. Thomas, K. Hatakeyama-Sato, S. Nanbu, M. Yoshizawa-Fujita, Organic ionic plastic crystals: flexible solid electrolytes for lithium secondary batteries, Energy Adv. 2 (2023) 748–764.
[5] D. Al-Masri, R. Yunis, A.F. Hollenkamp, C.M. Doherty, J.M. Pringle, The influence of alkyl chain branching on the properties of pyrrolidinium-based ionic electrolytes, Phys. Chem. Chem. Phys. 22 (2020) 18102–18113.
[6] W.A. Henderson, V.G. Young Jr, S. Passerini, P.C. Trulove, H.C. De Long, Plastic phase transitions in *N*-Ethyl-*N*-methylpyrrolidinium Bis(trifluoromethanesulfonyl) imide, Chem. Mater. 18 (2006) 934–938.
[7] K. Matsumoto, U. Harinaga, R. Tanaka, A. Koyama, R. Hagiwara, K. Tsunashima, The structural classification of the highly disordered crystal phases of $[N_n][BF_4]$, $[N_n][PF_6]$, $[P_n][BF_4]$, and $[P_n][PF_6]$ salts (N_n^+ = tetraalkylammonium and P_n^+ = tetraalkylphosphonium), Phys. Chem. Chem. Phys. 16 (2014) 23616–23626.
[8] H.-Y. Zhang, Y.-Y. Tang, P.-P. Shi, R.-G. Xiong, Toward the targeted design of molecular ferroelectrics: modifying molecular symmetries and homochirality, Acc. Chem. Res. 52 (2019) 1928–1938.
[9] J. Harada, T. Shimojo, H. Oyamaguchi, H. Hasegawa, Y. Takahashi, K. Satomi, Y. Suzuki, J. Kawamata, T. Inabe, Directionally tunable and mechanically deformable ferroelectric crystals from rotating polar globular ionic molecules, Nat. Chem. 8 (2016) 946–952.
[10] J. Harada, H. Takahashi, R. Notsuka, M. Takehisa, Y. Takahashi, T. Usui, H. Taniguchi, Ferroelectric ionic molecular crystals with significant plasticity and a low melting point: high performance in hot-pressed polycrystalline plates and melt-grown crystalline sheets, Angew. Chem. Int. Ed. 62 (2023).
[11] Z.-H. Wei, Z.-T. Jiang, X.-X. Zhang, M.-L. Li, Y.-Y. Tang, X.-G. Chen, H. Cai, R.-G. Xiong, Rational design of ceramic-like molecular ferroelectric by quasi-spherical theory, J. Am. Chem. Soc. 142 (2020) 1995–2000.
[12] M. Moskwa, E. Ganczar, P. Sobieszczyk, W. Medycki, P. Zieliński, R. Jakubas, G. Bator, Temperature-stimulus responsive ferroelastic molecular–ionic crystal: $(C_8H_{20}N)[BF_4]$, J. Phys. Chem. C 124 (2020) 18209–18218.
[13] J.-H. Lin, J.-R. Lou, L.-K. Ye, B.-L. Hu, P.-C. Zhuge, D.-W. Fu, C.-Y. Su, Y. Zhang, Halogen engineering to realize regulable multipolar axes, nonlinear optical response, and piezoelectricity in plastic ferroelectrics, Inorg. Chem. 62 (2023) 2870–2876.
[14] S. d'Agostino, L. Fornasari, D. Braga, Binary and ternary solid solutions of ionic plastic crystals, and modulation of plastic phase transitions, Cryst. Growth Des. 19 (2019) 6266–6273.
[15] M. Matsuki, T. Yamada, N. Yasuda, S. Dekura, H. Kitagawa, N. Kimizuka, Nonpolar-to-polar phase transition of a chiral ionic plastic crystal and switch of the rotation symmetry, J. Am. Chem. Soc. 140 (2018) 291–297.
[16] X. Lan, X. Wang, D.X. Zhang, T. Mu, X.Z. Lan, Cation and Anion Transfer in Quinuclidinium Hexafluorophosphate Plastic Crystal: role of Constituent Ions and the Crystalline Structure, J. Phys. Chem. C 125 (2021) 21169–21178.
[17] Y. Yamada, E. Kashimoto, H. Honda, New Chemical Family of $[n\text{-}C_xH_{(2x+1)}NEt_3][BEt_3Me]$ Showing Ionic Plastic-Crystal (x = 4, 5), Rotator-Crystal (x = 6, 7) and Liquid-Crystal Phases (x = 8–16), Bull. Chem. Soc. Jpn 92 (2019) 1289–1298.
[18] H. Zhou, S. Sato, Y. Nishiyama, G. Hatakeyama, X. Wang, Y. Murakami, T. Yamada, Molecular design of organic ionic plastic crystals consisting of tetracyanoborate with ultralow phase transition temperature, J. Phys. Chem. Lett. 14 (2023) 9365–9371.
[19] H. Honda, M. Kenmotsu, N. Onoda-Yamamuro, H. Ohki, S. Ishimaru, Y. Furukawab, R. Ikeda, ^{15}N and ^{133}Cs Solid NMR studies on ionic dynamics in plastic CsNO2, Z. Naturforsch A 51 (1996) 761–768.
[20] K. Nagai, Y. Ookubo, H. Honda, Solid-state ^{1}H and ^{13}C NMR studies of new ionic plastic-crystals with branched structures: $[NEtxMe_{(3-x)}(i\text{-}Pr)][BEt_{(4-y)}Me_y]$ (x = 1-3, y = 0, 1), Phys. Chem. Chem. Phys. 26 (2024) 29780–29787.
[21] S.L. Piper, L. Melag, M. Kar, A. Sourjah, X. Xiao, E.F. May, K.-F. Aguey-Zinsou, D. R. MacFarlane, J.M. Pringle, Organic ionic plastic crystals having colossal barocaloric effects for sustainable refrigeration, Science 387 (2025) 56–62.
[22] R.J. Webb, M.D. Lowery, Y. Shiomi, M. Sorai, R.J. Wittebort, D.N. Hendrickson, Ferrocenium hexafluorophosphate: molecular dynamics in the solid state, Inorg. Chem. 31 (1992) 5211–5219.
[23] F. Grepioni, G. Cojazzi, S.M. Draper, N. Scully, D. Braga, Crystal forms of hexafluorophosphate organometallic salts and the importance of charge-assisted C—H—F hydrogen bonds, Organometallics 17 (1998) 296–307.
[24] H. Schottenberger, K. Wurst, U.J. Griesser, R.K.R. Jetti, G. Laus, R.H. Herber, I. Nowik, ^{57}Fe-labeled octamethylferrocenium tetrafluoroborate. X-ray crystal structures of conformational isomers, hyperfine interactions, and spin-lattice relaxation by Moessbauer spectroscopy, J. Am. Chem. Soc. 127 (2005) 6795–6801.
[25] T. Mochida, M. Ishida, T. Tominaga, K. Takahashi, T. Sakurai, H. Ohta, Paramagnetic ionic plastic crystals containing the octamethylferrocenium cation: counteranion dependence of phase transitions and crystal structures, Phys. Chem. Chem. Phys. 20 (2018) 3019–3028.
[26] J. García-Ben, I. Delgado-Ferreiro, R.J.C. Dixey, S. Castro-García, J. López-Beceiro, R. Artiaga, M. Sánchez-Andújar, A.E. Phillips, J.M. Bermúdez-García, M.A. Señarís-Rodríguez, Unveiling barocaloric potential in organometallic-sandwich compounds $[Cp_2M][PF_6]$ (M: Fe^{3+}, Co^{3+}), J. Mater. Chem. A Mater. Energy Sustain 12 (2024) 23751–23760.
[27] T. Mochida, Y. Funasako, M. Ishida, S. Saruta, T. Kosone, T. Kitazawa, Crystal structures and phase sequences of metallocenium salts with fluorinated anions: effects of molecular size and symmetry on phase transitions to ionic plastic crystals, Chem. Eur. J 22 (2016) 15725–15732.
[28] H. Kimata, T. Sakurai, H. Ohta, T. Mochida, Phase transitions, crystal structures, and magnetic properties of ferrocenium ionic plastic crystals with CF_3BF_3 and other anions, ChemistrySelect 4 (2019) 1410–1415.
[29] H. Kimata, T. Mochida, Effects of molecular structure on phase transitions of ionic plastic crystals containing cationic sandwich complexes, Cryst. Growth Des. 18 (2018) 7562–7569.
[30] T. Mochida, Y. Funasako, T. Inagaki, M.-J. Li, K. Asahara, D. Kuwahara, Crystal structures and phase-transition dynamics of cobaltocenium salts with bis (perfluoroalkylsulfonyl)amide anions: remarkable odd-even effect of the fluorocarbon chains in the anion, Chem. Eur. J. 19 (2013) 6257–6264.
[31] T. Tominaga, T. Ueda, T. Mochida, Effect of substituents and anions on the phase behavior of Ru(II) sandwich complexes: exploring the boundaries between ionic liquids and ionic plastic crystals, Phys. Chem. Chem. Phys. 19 (2017) 4352–4359.
[32] H. Kimata, R. Sumitani, T. Mochida, Phase transitions and crystal structures of ionic plastic crystals comprising quaternary ammonium cations and carborane anion, Chem. Lett. 48 (2019) 859–862.
[33] Y. Nakazono, R. Inoue, R. Sumitani, T. Mochida, Ionic plastic crystals and ionic liquids containing quaternary cations with alkenyl substituents: chemical phase transformations by bromine vapor, New J. Chem. 48 (2024) 2219–2225.
[34] M. Moriya, T. Watanabe, W. Sakamoto, T. Yogo, Combination of organic cation and cyclic sulfonylamide anion exhibiting plastic crystalline behavior in a wide temperature range, RSC Adv. 2 (2012) 8502–8507.
[35] A.L. Rohl, D.M.P. Mingos, Size and shape of molecular ions and their relevance to the packing of the 'soft salts,', Inorganica Chim. Acta 212 (1993) 5–13.
[36] P. Atkins, T. Overton, J. Rourke, M. Weller, F, Shriver and Atkins' Inorganic Chemistry, Oxford University Press, Oxford, 2010.
[37] D.K. McLemore, D.A. Dixon, S.H. Strauss, Density functional theory and fluorocarboranes, Inorg. Chim. Acta 294 (1999) 193–199.
[38] R. Inoue, R. Sumitani, T. Mochida, Preparation, Thermal properties, and structures of ionic plastic crystals with sandwich and half-sandwich Ru complexes, J. Organomet. Chem. 1013 (2024) 123162.

[39] R. Inoue, R. Sumitani, H. Honda, D. Kuwahara, Z.L. Goo, K. Sugimoto, T. Mochida, Organometallic ionic plastic crystals incorporating cationic half-sandwich complexes, Inorg. Chem. 63 (2024) 14770–14778.
[40] G.M. Sheldrick, A short history of SHELX, Acta Crystallogr. A 64 (2008) 112–122.
[41] O.V. Dolomanov, L.J. Bourhis, R.J. Gildea, J.A.K. Howard, H. Puschmann, *OLEX2*: a complete structure solution, refinement and analysis program, J. Appl. Crystallogr. 42 (2009) 339–341.
[42] G.M. Sheldrick, SHELXT - integrated space-group and crystal-structure determination, Acta Crystallogr. A 71 (2015) 3–8.
[43] G.M. Sheldrick, Crystal structure refinement with SHELXL, Acta Crystallogr. C 71 (2015) 3–8.